Charge confinement and thermal transport processes in modulation-doped epitaxial crystals lacking lattice interfaces

Elizabeth Radue, Evan L. Runnerstrom, Kyle P. Kelley, Christina M. Rost, Brian F. Donovan, Everett D. Grimley, James M. LeBeau, Jon-Paul Maria, and Patrick E. Hopkins

Phys. Rev. Materials **3**, 032201 — Published 29 March 2019

DOI: 10.1103/PhysRevMaterials.3.032201

Charge Confinement and Thermal Transport Processes in Modulation-Doped Epitaxial Crystals (MoDECs) Lacking Lattice Interfaces

Elizabeth Radue[1], Evan L. Runnerstrom[2,3], Kyle P. Kelley[2,3], Christina M. Rost[1], Brian F. Donovan,[4] Everett D. Grimley[2], James M. LeBeau[2], Jon-Paul Maria[2,3], Patrick E. Hopkins[1,5,6,*]

1. Department of Mechanical and Aerospace Engineering, University of Virginia, Charlottesville, VA 22904, USA
2. Department of Materials Science, North Carolina State University, Raleigh, NC 27695, USA
3. Department of Materials Science and Engineering, Penn State University, State College, PA 16801, USA
4. Department of Physics, United States Naval Academy, Annapolis, MD 21402, USA
5. Department of Materials Science and Engineering, University of Virginia, Charlottesville, VA 22904, USA
6. Department of Physics, University of Virginia, Charlottesville, VA 22904, USA

Dr. E. Radue, Dr. C.M. Rost, Prof. P.E. Hopkins
Department of Mechanical Engineering and Aerospace Engineering
University of Virginia
122 Engineers Way, Charlottesville, VA 22904 USA

Dr. E.L. Runnerstrom, Prof. J. P. Maria
Department of Materials Science and Engineering
Penn State University
215 Steidle Building, University Park, PA 16802

Dr. E. D. Grimley, Prof. J. M. LeBeau
Department of Materials Science and Engineering
911 Partners Way FB I
Raleigh, NC 27695, USA

Prof. B.F. Donovan
United States Naval Academy
Department of Physics
572c Holloway Road, Annapolis, MD 21402

*Author to whom correspondence should be addressed: phopkins@virginia.edu

Abstract

Heterogeneous nanosystems offer a robust potential for manipulating various functional material properties, beyond those possible of their individual constituent materials. We demonstrate the formation of a new class of materials with a homogeneous lattice but spatially heterogeneous electrical functionality; specifically, we develop epitaxial modulation-doped thin films in which the spatial separation of electronic charge densities is achieved without perturbing the parent crystal's compositional or structural homogeneity. Unlike the previous realizations of modulation doping in crystals, our materials demonstrate periodic layering of spatially segregated, varying electronically donor-doped regions in a single compositionally and structurally homogenous single crystalline lattice. We demonstrate the formation of "Modulation-Doped Epitaxial Crystals" (MoDECs) using alternating layers of doped cadmium oxide, and the ability to spatially confine regions of variable carrier concentration via low potential energy barriers in a spatially homogeneous, epitaxial crystal with a chemically and structurally homogenous lattice (i.e., no chemical or structural lattice interfaces). The low potential energy that confines electrons within the doped layers coupled with the crystalline nature of the MoDECs and lack of lattice interfaces presents an unprecedented platform to study the electron thermal boundary resistances at low energy electronic barriers. We find that the electron interfacial density does not impede thermal conductivity, despite evidence that the doped layers retain their carrier concentrations. Thus, the negligible thermal boundary resistances at the electronic interfaces result in the thermal conductivities of the MoDECs being related to only a series resistance sum of the thermal resistances of each of the individual layers, with no thermal resistances from the electronic boundaries that maintain charge separation. This is in stark contrast with other nanoscale multilayer materials, where thermal boundary resistances at the internal material interfaces reduce the thermal conductivity of the multilayer compared to that of the parent materials. The ability to modulation dope epitaxially grown films with no structural heterogeneity in the lattice will further enable unique platforms for mid-IR photonics, such as hyperbolic metamaterials, optical filters with spatially-discrete optical absorption, or energy harvesting based on charge injection across modulation-doped interfaces.

Keywords

Electron and phonon thermal conductivity, electron energy barrier, modulation doping, modulation-doped epitaxial crystals (MoDECs), thermal boundary resistance

Superlattices and other periodic material multilayers are arguably the some of the most studied nanostructures in terms of their functional properties. This unique class of nanomaterials has attracted considerable attention over the past few decades since they provide the ability to manipulate material properties at the length scales of the fundamental carriers of energies. For example, the periodic patterning of alternating non-metals and/or metals, with periodicities on the order of nanometers to micrometers, has led to impeccable control over photon, electron and/or phonon transport that has resulted in promising solutions for thermoelectric devices,[1,2] quantum cascade and vertical cavity surface emitting laser diodes,[3-6] amplified photodetectors,[7-11] and radiation resistant coatings.[12,13]

Along these lines, the electronic and thermal transport properties of superlattices have been of fundamental interest to study unique properties of electrons and phonons. For example, researchers have used metal-metal superlattices to validate the Wiedemann-Franz Law at interfaces,[14] and demonstrate the exceptionally large electron-electron thermal boundary conductance across metal/metal interfaces.[12,13] In non-metal/non-metal superlattices, a wealth of studies have demonstrated the strong reduction in thermal conductivity that can occur due to phonon-boundary scattering,[15-20] while more recent works have experimentally demonstrated a combination of ballistic and coherent phononic transport that can occur in these periodic structures,[5,20] along with the existence of a minimum in the thermal conductivity as a function of period thickness.[21] These unique phonon processes, the observation of which is enabled by the nanoscale design of the superlattices, provide evidence of mini-band formation and shed insight into the wave-particle duality of phonons.[22]

A more multi-functional form of compositionally layered semiconductor systems requires judicious doping of the semiconductor layers in constructing tailored photonic interactions or electronic transport. In particular, modulation doping of individual material layers in these superlattices, which leads to spatial separation of free carriers,[23,24] has demonstrated the potential for improved functionality, such as an increased thermoelectric response using modulation-doped superlattices.[25] Moving beyond compositionally heterogeneous layered structures, modulation doping has been realized in 3D solid solutions by varying cation compositions (e.g., $(Bi_xSn_{1-x}Se)_{1+\delta}TiSe_2$)[26] or by creating two-phase composites with doped and undoped nanoregions (e.g., BiCuSeO and $Bi_{0.75}Ba_{0.25}CuSeO$, or SiGe and Si).[27-29] In the former of these cases, the anisotropy, orientation, and natural layering of the crystalline unit cell enabled modulation doping, where in the latter case, lattice interfaces between the two phases in the three-dimensional matrix facilitated carrier segregation. In the case of modulation-doped BiCuSeO/$Bi_{0.75}Ba_{0.25}CuSeO$ composites,[27] the sample is actually a two-phase composite with the modulation doping enabled by carrier delocalization across the grain boundaries (i.e., crystalline disorder) separating the BiCuSeO matrix and the $Bi_{0.75}Ba_{0.25}CuSeO$ inclusions. In fact, all previous modulation-doped materials required interfaces and boundaries in the crystalline lattice (e.g., interfaces in superlattices, anisotropy in layered compounds, and phase boundaries in nanocomposites) to ensure that the free carrier regions are both spatially and chemically separated from the donor regions or regions with lower carrier concentrations. Modulation doping in a high-quality single crystal with a structurally and chemically homogeneous lattice with only spatially varying *charge* has never been realized, to the best of our knowledge.

Here, we report on the charge and heat transport processes in a new class of epitaxial modulation-doped thin films in which the spatial separation of electronic charge densities is achieved without perturbing the parent crystal's compositional or structural homogeneity. Unlike the previous realizations of modulation doping in crystals, our materials demonstrate periodic layering of spatially segregated, varying electronically donor-doped regions in a single compositionally and structurally homogenous single crystalline lattice; in other words, while these modulation-doped single lattice films contain discrete and sharp *electronic* boundaries, they do not contain any *morphological or chemical* boundaries or interfaces in the lattice. Thus, we refer to these modulation-doped nanomaterials as "Modulation-Doped Epitaxial Crystals" (MoDECs).

We demonstrate the formation of MoDECs using superlattices comprised of alternating layers of yttrium-doped and intrinsic (unintentionally/oxygen vacancy-doped) cadmium oxide (Y:CdO and i-CdO, respectively). The small electronic potential that confines electrons within the doped layers, coupled with the epitaxial and crystalline nature of the MoDECs and lack of lattice interfaces, presents an unprecedented platform to study charge transport and the electron thermal boundary resistances across electronic interfaces. It is well known that structural boundaries in an otherwise crystalline lattice or interfaces between chemically dissimilar crystals can give rise to phonon scattering events and phonon thermal boundary resistances that reduce the thermal conductivity of the composite material.[15,30-36] In our MoDECs, with an order of magnitude electronic contrast between each layer, but less than 1% chemical contrast, these phonon-phonon interfacial resistances are nominally absent, offering unimpeded phonon thermal conductivity in these single crystalline systems. We note that doping CdO leads to an increase in electronic

thermal conductivity and a corresponding decrease in the phonon contribution to thermal conductivity.[37] The thermal conductivity of intrinsic CdO is dominated by phonon transport with only a minor contribution from electrons.[37] While increasing the dopant concentration in CdO to improve the electronic-based functionality will reduce the phonon contribution to thermal conductivity, this phononic contribution can still play a non-negligible role in heat conduction, depending on the atomic densities of the dopant atoms.[37] Thus, phonon conduction that is unimpeded by interfaces can offer improved temperature regulation and thermal management in devices based on MoDECs.

However, given the presence an electronic superlattice with periodically varying carrier concentration and electronic mobility, a question arises: do these electronic interfaces impede electronic and/or thermal transport, and what are the primary heat transport processes that dictate the thermal conductivity of MoDECs? Given that both the i-CdO and Y:CdO constituents have fairly high electronic conductivity, the thermal conductivities of i-CdO/Y:CdO MoDECs are expected to contain significant electronic contributions.[37] Here, we aim to determine if the electric potential that confines electrons within the Y:CdO layers presents additional electronic or thermal resistances to the overall material. We not only find that i-CdO and Y:CdO layers are perfectly electronically coupled, but also that modulation doping enhances electronic mobility within one or both constituents by up to 15%. Our analysis further suggests that the thermal boundary resistances across the low potential energy electronic interfaces are negligible, and the thermal conductivity of MoDECs are controllable based on the electronic thermal conductivities of the doped layers comprising the sample. The thermal conductivities of the MoDECs samples range from ~8 – 12 W m^{-1} K^{-1}, depending on volume fraction of the yttrium doped cadmium

oxide in the MoDECs. These thermal conductivities can be described from a series resistance model of the diffusive thermal resistances of the parent materials comprising the individual layers of the MoDECs, with negligible influence of the thermal boundary resistances at the electronic i-CdO/Y:CdO interfaces.

To the best of our knowledge, nanoscale multilayer films made up of parent materials that have notably different transport properties yet composite thermal conductivities that exhibit negligible influences from the thermal boundary resistances at the internal interfaces have never been previously realized.[16] Indeed, even in the case of metal/metal multilayers, where thermal boundary resistances at the metal/metal interfaces are some of the lowest values ever measured for solid/solid interfaces (~ 0.07 – 0.25 m^2 K GW^{-1}), the thermal conductivities of the metal/metal composites are substantially reduced compared to the thermal conductivities of the parent materials comprising the multilayers.[12-14] This marks a unique thermophysical property of the MoDECs that is enabled by the lack of lattice interfaces, yet electronic potential barriers that can maintain spatial charge segregation via an interface with negligible impact on thermal transport (i.e., negligible thermal boundary resistances).

We recently demonstrated that doped-CdO thin films exhibit strong, tunable, and low-loss plasmonic absorption in the mid-IR thanks to their exceptionally high electronic motilities,[38,39] offering unique opportunities for mid-IR plasmonic and photonic devices. Modulation-doped CdO systems will further enable unique platforms for mid-IR photonics, such as hyperbolic metamaterials,[40,41] optical filters with spatially-discrete optical absorption,[42,43] or energy harvesting based on charge injection across modulation-doped interfaces.[28]

We grew i-CdO/Y:CdO superlattices on r-plane (012) sapphire at 455 °C *via* reactive high impulse power magnetron sputtering (HiPIMS) of a 2-inch pure metallic Cd (99.9999%) target in a mixed Ar/O_2 atmosphere (20/14.4 sccm, 10 mTorr). Doping was achieved by applying RF (13.56 MHz) power to a 2" metallic yttrium target affixed to a magnetron sputtering source to achieve a target nominal yttrium dopant concentration of $n = 2.1x10^{20}$ cm^{-3} in the CdO. To grow MoDECs, we first deposited a heteroepitaxial i-CdO or Y:CdO layer with thickness controlled by deposition rate as calibrated by x-ray reflectivity (XRR). The subsequent alternating doped/intrinsic superlattice layers were grown homoepitaxially, with thickness controlled by calibrated sputtering rates, and doping controlled by a shutter on the yttrium source. Following deposition, the samples were annealed at 700°C under 1 atm O_2 for 30 minutes to maximize oxygen uptake. X-ray diffraction (XRD) symmetric 2θ-ω scans and rocking curves (**Fig. 1a-b**) confirm that the MoDECs are indeed epitaxial/crystalline, with crystalline quality directly comparable to i-CdO and Y:CdO monolayer reference samples. Annular dark-field scanning transmission electron microscopy (ADF STEM) of a modulation-doped sample, grown on c-plane (0001) sapphire, finds no evidence for structural changes induced by dopant layering in sputtered CdO films. In the low magnification ADF STEM image **Fig. 1c**, a vertically-oriented white bar of length 20 nm is centered on the position where doping transitions from i:CdO to Y:CdO, though this leads to no identifiable changes in image. A higher magnification micrograph acquired in the region marked with the black overlay shows no discernable changes in the atomic-scale structuring of the CdO lattice across the interface. This is consistent with our previous work,[44] where we show that the addition of Y-doping in CdO films has minimal effect on both the in- and out-of-plane lattice parameters of CdO. Furthermore, from our XRD data in

Fig. 1, we determine a lattice parameter in our samples of 4.694 Å, within 0.05% of the bulk lattice constant of CdO,[45] and within our experimental uncertainty. Additionally, the overlapping rocking curves of the various MoDECs and reference CdO films in Fig. 1b suggest that the MoDECs are crystallographically indistinguishable from the homogeneous reference films. This suggests that the Y-doping and varying modulation periods of the doped layers have negligible impact on the lattice of the films, and that our samples are strain relaxed.

Here, we study MoDECs with 2, 3, 5, 9, or 18 alternating layers, which corresponds to interface densities of 0.0056 nm^{-1}, 0.011 nm^{-1}, 0.022 nm^{-1}, 0.044 nm^{-1}, and 0.094 nm^{-1}, respectively. The total thickness of each MoDECs is nominally 180 nm, with the thickness of the constituent layers controlled so that total volume of i-CdO and Y:CdO is constant across each MoDECs sample set. We grew three different sample sets, with i-CdO to Y:CdO thickness ratios of 1:3, 1:1, and 3:1, hereafter referred to as $(CdO)_{0.25}/(Y:CdO)_{0.75}$, $(CdO)_{0.5}/(Y:CdO)_{0.5}$, and $(CdO)_{0.75}/(Y:CdO)_{0.25}$. **Table 1** contains further description of each MoDECs, including the nominal thickness of each layer. We additionally grew two 180 nm-thick single layer thin films of i-CdO (n = 1.9x10^{19} cm^{-3}; μ = 355 $cm^2/V{\cdot}s$) and Y:CdO (n = 2.1x10^{20} cm^{-3}; μ = 423 $cm^2/V{\cdot}s$) as reference samples, where n is the carrier density and μ is the mobility. Prior to measuring the thermal conductivity of each sample, we deposited 80 nm of Al on the film surface using electron beam evaporation. The overall thicknesses of each sample and the Al transducer were measured using XRR.

We quantified the electronic properties of each sample *via* Hall Effect measurements. **Figure 2a** shows that all of the MoDECs samples are conductive, with well-delineated conductivities that are similar to the conductivity of single layers grown with the equivalent average carrier

concentration of the MoDEC, i.e., the $(CdO)_{0.25}/(Y:CdO)_{0.75}$ samples have a nominal average n = $0.25(1.9x10^{19}\ cm^{-3}) + 0.75(2.1x10^{20}\ cm^{-3}) = 1.5x10^{20}\ cm^{-3}$. Notably, the electronic conductivity of each MoDECs is clearly *enhanced* relative to single layer films, especially in the 3- to 9-layer superlattices. Hall effect measurements reveal that this conductivity enhancement arises primarily from an increased overall electronic mobility in multilayer samples, while the carrier concentration follows the law of averages. Based on a multilayer model for Hall effect measurements (Supplemental Material),[46] this effect is a clear signature of strong electronic coupling between the i-CdO and Y:CdO layers, with negligible resistance at the electronic interface.[47,48] Furthermore, our multilayer electronic model shows that the increased mobility measured over the full MoDECs stacks can only be explained by either a simultaneous mobility enhancement of up to 17% across both of the i-CdO/Y:CdO constituents, or a mobility enhancement of up to 68% within one constituent. Considering that the mobility enhancement is greatest in the $(CdO)_{0.75}/(Y:CdO)_{0.25}$ samples, we speculate that through modulation doping, Y:CdO layers donate electrons to the i-CdO layers in the vicinity of the electronic interface to neutralize ionized point defects; our model predicts an effective 68% mobility increase within the i-CdO layers from 355 $cm^2/V{\cdot}s$ to 596 $cm^2/V{\cdot}s$ in the most extreme case. While microscopic evidence for this hypothesis is beyond the scope of this report, a similar effect, with a four-fold mobility increase, has already been observed at SnTe/CdO interfaces.[47] Finally, finite-element simulations (COMSOL Multiphysics®, **Fig. 2b**) of Poisson's equation in i-CdO/Y:CdO MoDECs confirm that electronic charge is localized within individual layers in our MoDECs films. Because of the large and degenerate electron concentrations throughout the MoDECs thickness, and because the electron concentration of the Y:CdO layers is more than an order of magnitude larger than in the i-CdO layers, the depletion/accumulation regions in the superlattices

is exceptionally short, on the order of 1 – 5 nm. Thus, over the thickness of the MoDECs, the carrier concentration is expected to have a strongly localized box-like profile. The 18-layered MoDECs are an important exception, as the layers become thin enough that the depletion/accumulation lengths are comparable to the layer thickness (Supplemental Material).[46] Importantly, IR-reflectivity measurements of our MoDECs, along with Drude model-based fits using the transfer matrix method, allowed us to experimentally confirm charge separation and rule out dopant/carrier intermixing by diffusion (Supplemental Material).[46]

We measured the thermal conductivities of each MoDEC using Time Domain Thermoreflectance (TDTR).[12,32,49-51] Details of our TDTR measurements and analysis are found in the Supplemental Material.[46] The thermal conductivities of the CdO-based MoDECs and calibration films are shown in **Fig. 2c**. We note that all thermal conductivities reported in this work represent the thermal conductivity in the cross-plane direction, perpendicular to the interfaces.

We measure the cross-plane thermal conductivity of the intrinsic and doped CdO control films as 8.2 and 12.1 W m^{-1} K^{-1}, respectively. Using the Wiedemann-Franz law applied to our in-plane electrical conductivity measurements (**Fig. 2a**), we then estimate the in-plane electron thermal conductivity of the i-CdO and Y:CdO films as 0.8 and 10.4 W m^{-1} K^{-1}, respectively. Thus, this suggests that the thermal transport in the intrinsic layers are primarily dominated by phonon conduction, where electrons contribute to the majority of thermal conductivity in the doped layers (i.e., >80% of the total thermal conductivity is from electrons in the doped layers). This is consistent with our previous findings on Dy-doped CdO.[37] Given the cubic symmetry of CdO and ability to separate the influence of film/substrate interfaces from the intrinsic cross-plane

thermal conductivity of these CdO films, comparing the in-plane-derived electron thermal conductivity to the TDTR-measured total thermal conductivity is acceptable for estimating the relative electron and phonon contributions to thermal conductivity.

The general trend among all MoDEC samples is that the thermal conductivity changes with increasing interface density relative to the i-CdO and Y:CdO controls up to about 0.02 interfaces/nm, at which point the thermal conductivity is relatively constant. However, the way in which the thermal conductivity changes with interface density depends on the relative thicknesses of the doped and undoped layers. For example, increasing interfacial density reduces the thermal conductivity of the $(CdO)_{0.25}/(Y:CdO)_{0.75}$ samples relative to the Y:CdO control. Conversely, the thermal conductivity is higher in the $(CdO)_{0.75}/(Y:CdO)_{0.25}$ and $(CdO)_{0.50}/(Y:CdO)_{0.50}$ samples relative to the intrinsic CdO control. Above an interface density of 0.02 interfaces/nm, the thermal conductivities of the $(CdO)_{0.75}/(Y:CdO)_{0.25}$ and $(CdO)_{0.50}/(Y:CdO)_{0.50}$ are relatively similar and lower than that of the $(CdO)_{0.25}/(Y:CdO)_{0.75}$.

In previous works studying the thermal conductivity of multilayers and superlattices, the thermal conductivities of these systems are always lower than those of the individual materials that comprise the structures. For example, in Cu/Nb and Pt/Ir multilayers, the thermal conductivities are less than that of Cu and Nb, or Pt and Ir, respectively.[13,14] This is due to the electron thermal boundary resistances at the metal/metal interfaces that drive down the total thermal conductivity of the multilayers films.[13,52,53] The same holds true with metal/nonmetal[54-56] and non-metal/non-metal[5,16,19,21,57] superlattices, where in these cases the phonon thermal boundary resistances typically play the dominant resistor role. In the case of our MoDECs, we see a different trend:

simply increasing the volume fraction of the higher thermal conductivity material that comprises the MoDEC leads to an increase in thermal conductivity. This implies that any potential interfacial resistances in the electronic or phononic sub-systems in the MoDECs are negligible (i.e., electron-electron, electron-phonon, phonon-phonon).

To test this hypothesis, we measured the thermal conductivity of a series of films with equivalent carrier densities as the average carrier concentrations in the MoDEC films, as they should have an equivalent contribution from the carriers, without any potential barriers from the electronic interfaces. **Figure 3** shows the thermal conductivity of the Y:CdO films as a function of average carrier density in the CdO. In line with our previous experiments, the thermal conductivity of the CdO increases with carrier density due to an increase in the electronic contribution to thermal conductivity.[37,38] Also shown in Fig. 3 are the thermal conductivities of the MoDECs samples from Fig. 2 plotted as a function of average carrier density across the entire sample thickness. We determine the carrier densities of the MoDECs by performing a weighted average of the carrier concentrations of the yttrium doped and intrinsic regions based on the volume fraction of each layer. The thermal conductivities of these MoDECs are calculated by averaging the thermal conductivity data in **Fig. 2** over all samples with an interface density greater than or equal to 0.02 interfaces/nm, where the error bars represent the standard deviation among these data.

The similarities between the MoDEC samples and the single-layer samples with equivalent carrier densities suggest that the electronic interfaces that exist between the Y-doped and intrinsic CdO layers do not pose any appreciable resistance to heat transport. Furthermore, as previously mentioned, since there are no lattice interfaces or changes in crystallinity in the

MoDEC samples, a phonon thermal boundary resistance does not exist in these samples. Thus, our experimental data suggest that the thermal conductivities of these MoDECs are driven by parallel phononic and electronic contributions, with the electronic portion dictated by the summation of the electronic contributions in both the intrinsic and yttrium-doped layers.

To support this conclusion, we model the thermal conductivity of the MoDECs using a series thermal resistance approach, where

$$\kappa_{MoDSiLF} = \frac{d_{total}}{R_{total}} = (R_{Y:CdO} + R_{i-CdO} + R_{int})^{-1} \quad (1)$$

where d_{total} is the total thickness of the MoDEC and R_{total} is its thermal resistance of the MoDEC sample, $R_{Y:CdO}$ is the thermal resistance of the yttrium-doped CdO layer, $R_{i\text{-}CdO}$ is the thermal resistance of the intrinsic CdO layer, and R_{int} is the thermal boundary resistance at the Y:CdO/i-CdO interface; this model is graphically depicted in **Fig. 3a**. From our previous discussion, we assume $R_{int} = 0$, thus Eq. (1) becomes

$$\kappa_{MoDSiLF} = (R_{Y:CdO} + R_{i-CdO})^{-1} = \left(\frac{d_{Y:CdO}}{\kappa_{Y:CdO}} + \frac{d_{i-CdO}}{\kappa_{i-CdO}}\right)^{-1} \quad (2)$$

where d is the total thickness of the Y:CdO or i-CdO layers in the sample. Calculations of Eq. (2) are shown in **Fig. 3** (solid blue line), where we assume $\kappa_{Y:CdO}$ = 12.0 ± 1.7 W m^{-1} K^{-1} and $\kappa_{i\text{-}CdO}$ = 8.3 ± 0.9 W m^{-1} K^{-1} from the calibrations shown in **Fig. 2**; the dashed lines are the calculations of Eq. (2) when accounting for the uncertainty in $\kappa_{Y:CdO}$ and $\kappa_{i\text{-}CdO}$. The agreement between our model calculations and experimental data on the MoDEC support our hypothesis that $R_{int} = 0$. Thus, in our MoDEC, the series contribution to the thermal conductivity of the electrons from each layer behave as isolated resistors, and the sum of all the resistors dictate the overall resistance of the structure, with negligible resistance from the potential barrier at the Y:CdO/i-CdO interface. Stated differently, a rule of mixtures adequately describes the overall

thermal resistance of the MoDEC, similar to the heat transport processes in more traditionally studied superlattices.

Based on our discussion above, we can estimate a maximum resistance associated with the electronic potential barrier at the Y:CdO/i-CdO interface. In the highest interface density samples, the average thicknesses of the Y:CdO and i-CdO layers are 10 nm. This corresponds to thermal resistances of each layer of $R_{Y:CdO} = 10x10^{-9}/\kappa_{Y:CdO} = 0.8$ m^2 K GW^{-1} and $R_{i\text{-}CdO} = 10x10^{-9}/\kappa_{i\text{-}CdO} = 1.2$ m^2 K GW^{-1}, yielding a MoDEC resistance of 2.0 m^2 K GW^{-1}. To yield a non-negligible change in total resistance of the MoDEC, which we assume as a ~18% change based on the uncertainties reported in our calculations of Eq. (2) and shown in Fig. 3b, the thermal resistances at the Y:CdO/i-CdO interfaces must be greater than $R_{int} > 0.4$ m^2 K GW^{-1} (rounding up based on precision). Thus, we estimate that the maximum possible thermal resistance at these Y:CdO/i-CdO interfaces is 0.4 m^2 K GW^{-1}. Stated differently, the lowest possible electron thermal boundary conductance across the electronic potential barrier formed at the Y:CdO/i-CdO interface is 2.5 GW m^{-2} K^{-1}, a relatively high thermal boundary conductance that is typical for interfaces between two regions of different electronic carrier concentration, and consistent with prior works studying the thermal boundary conductance across metal/metal interfaces.[12-14]

In summary, we have demonstrated the formation of a new class of epitaxial modulation-doped thin films in which the spatial separation of electronic charge densities is achieved without perturbing the parent crystal's compositional or structural homogeneity. Unlike the previous realizations of modulation doping in crystals, our materials demonstrate periodic layering of spatially segregated, varying electronically donor-doped regions in a single compositionally and

structurally homogenous single crystalline lattice. We form these "Modulation-Doped Epitaxial Crystals" (MoDECs) using alternating layers of doped/intrinsic cadmium oxide, and from this, our work demonstrates the ability to spatially confine regions of variable carrier concentration via low potential energy barriers in a spatially homogeneous, single crystal with a chemically and structurally homogenous lattice (i.e., no chemical or structural lattice interfaces). The low potential energy that confines electrons within the doped layers coupled with the single crystal nature of the MoDECs and lack of lattice interfaces presents an unprecedented platform to study the electron thermal boundary resistances at low energy electronic barriers. We measure the cross plane thermal conductivity of an array of MoDECs with different electronic interfaces densities and assess the various heat transport mechanisms, including the role of the electronic interfaces separating the variably-doped regions. We find that any potential thermal boundary resistances in the electronic or phononic sub-systems in the MoDECs are negligible, the series contribution to thermal conductivity of the electrons from each layer behave as isolated resistors, and the sum of all the resistors dictate the overall thermal resistance of the structure with negligible resistance from the potential barrier at the Y:CdO/i-CdO interface. This is in stark contrast with other nanoscale multilayer materials, where thermal boundary resistances at the internal material interfaces reduce the thermal conductivity of the multilayer compared to that of the parent materials. This marks a unique thermophysical property of the MoDECs that is enabled by the lack of lattice interfaces, yet electronic potential barriers that can maintain spatial charge segregation via an interface with negligible impact on thermal transport (i.e., negligible thermal boundary resistances). Based on the resistances of the individual layers in the MoDECs, we estimated the maximum possible thermal boundary resistance as 0.4 m^2 K GW^{-1} (or a minimum possible thermal boundary conductance 2.5 GW m^{-2} K^{-1}), ensuring that the thermal

resistance across the electronic potential barrier remains relatively negligible as compared to the thermal resistances of the layers in the MoDECs. This low value of electron-electron thermal boundary resistance is consistent with those measured across metal/metal interfaces. The ability to modulation dope these MoDECS systems and systematically tune their thermal resistances will further enable unique platforms for mid-IR photonics, such as hyperbolic metamaterials, optical filters with spatially-discrete optical absorption, or energy harvesting based on charge injection across modulation-doped interfaces.

Acknowledgements

We appreciate funding from the Army Research Office, Multidisciplinary University Research Initiative, Grant No. W911NF-16-1-0406. EDG and JML gratefully acknowledge support from the National Science Foundation (DMR-1350273). EDG acknowledges support for this work through a National Science Foundation Graduate Research Fellowship (DGE-1252376). This work was performed in part at the Analytical Instrumentation Facility (AIF) at North Carolina State University, which is supported by the State of North Carolina and the National Science Foundation (ECCS-1542015). The AIF is a member of the North Carolina Research Triangle Nanotechnology Network (RTNN), a site in the National Nanotechnology Coordinated Infrastructure (NNCI).

References

1. A. J. Minnich, M. S. Dresselhaus, Z. F. Ren and G. Chen, "Bulk nanostructured thermoelectric materials: current research and future prospects," *Energy and Environmental Science* **2**, 466-479 (2009).
2. M. Zebarjadi, K. Esfarjani, M. S. Dresselhaus, Z. F. Ren and G. Chen, "Perspectives on thermoelectrics: from fundamentals to device applications," *Energy and Environmental Science* **5**, 5147-5162 (2012).
3. A. D. Rakic, A. B. Djurisic, J. M. Elazar and M. L. Majewski, "Optical properties of metallic films for vertical-cavity optoelectronic devices," *Applied Optics* **37**, 5271-5283 (1998).
4. S. Clark, P. Ahirwar, F. Jaeckel, C. Hains, A. Albrecht, P. Schjetnan, T. J. Rotter, L. R. Dawson, G. Balakrishnan, P. E. Hopkins, L. M. Phinney, J. Hader and J. V. Moloney, "Growth and thermal conductivity analysis of polycrystalline GaAs on CVD diamond for use in thermal management of high-power semiconductor lasers," *Journal of Vacuum Science and Technology B* **29**, 03C130 (2011).
5. R. Cheaito, C. A. Polanco, S. Addamane, J. Zhang, A. W. Ghosh, G. Balakrishnan and P. E. Hopkins, "Interplay between total thickness and period thickness in the phonon thermal conductivity of superlattices from the nanoscale to the microscale: Coherent versus incoherent phonon transport," *Physical Review B* **97**, 085306 (2018).
6. G. Chen and C. L. Tien, "Facet heating of quantum well lasers," *Journal of Applied Physics* **74**, 2167-2174 (1993).
7. Q. Zhou, A. S. Cross, Y. Fu, A. Beling, B. M. Foley, P. Hopkins and J. C. Campbell, "Balanced InP/InGaAs Photodiodes With 1.5-W Output Power," *Photonics Journal, IEEE* **5**, 6800307 (2013).
8. Q. Zhou, A. S. Cross, F. Yang, A. Beling and J. C. Campbell, "Development of narrowband modified uni-travelling-carrier photodiodes with high power efficiency," *2013 IEEE Avionics, Fiber-Optics and Photonics Conference* **AVFOP**, 65-66 (2013).
9. M. Ren, S. Maddox, Y. Chen, M. Woodson, J. C. Campbell and S. Bank, "AlInAsSb/GaSb staircase avalanche photodiode," *Applied Physics Letters* **108**, (2016).
10. M. E. Woodson, M. Ren, S. J. Maddox, Y. Chen, S. R. Bank and J. C. Campbell, "Low-noise AlInAsSb avalanche photodiode," *Applied Physics Letters* **108**, 081102 (2016).
11. Y. Shen, J. T. Gaskins, X. Xie, B. M. Foley, R. Cheaito, P. E. Hopkins and J. C. Campbell, "Thermal analysis of high-power flip-chip-bonded photodiodes," *Journal of Lightwave Technology* **35**, 4242-4246 (2017).
12. R. Cheaito, C. S. Gorham, A. Misra, K. Hattar and P. E. Hopkins, "Thermal conductivity measurements via time-domain thermoreflectance for the characterization of radiation induced damage," *Journal of Materials Research* **30**, 1403-1412 (2015).
13. R. Cheaito, K. Hattar, J. T. Gaskins, A. K. Yadav, J. C. Duda, T. E. Beechem, J. F. Ihlefeld, E. S. Piekos, J. K. Baldwin, A. Misra and P. E. Hopkins, "Thermal flux limited electron Kapitza conductance in copper-niobium multilayers," *Applied Physics Letters* **106**, 093114 (2015).
14. R. B. Wilson and D. G. Cahill, "Experimental Validation of the Interfacial Form of the Wiedemann-Franz Law," *Physical Review Letters* **108**, 255901 (2012).

15. D. G. Cahill, W. K. Ford, K. E. Goodson, G. D. Mahan, A. Majumdar, H. J. Maris, R. Merlin and S. R. Phillpot, "Nanoscale thermal transport," *Journal of Applied Physics* **93**, 793-818 (2003).
16. P. M. Norris, N. Q. Le and C. H. Baker, "Tuning phonon transport: From interfaces to nanostructures," *Journal of Heat Transfer* **135**, 061604 (2013).
17. G. Chen, "Size and interface effects on thermal conductivity of superlattices and periodic thin-film structures," *Journal of Heat Transfer* **119**, 220-229 (1997).
18. G. Chen, "Thermal conductivity and ballistic-phonon transport in the cross-plane direction of superlattices," *Physical Review B* **57**, 14958-14973 (1998).
19. G. Chen, *Nanoscale Energy Transport and Conversion: A Parallel Treatment of Electrons, Molecules, Phonons, and Photons* (Oxford University Press, New York, 2005).
20. M. N. Luckyanova, J. Garg, K. Esfarjani, A. Jandl, M. T. Bulsara, A. J. Schmidt, A. J. Minnich, S. Chen, M. S. Dresselhaus, Z. Ren, E. A. Fitzgerald and G. Chen, "Coherent Phonon Heat Conduction in Superlattices," *Science* **338**, 936-939 (2012).
21. J. Ravichandran, A. K. Yadav, R. Cheaito, P. B. Rossen, A. Soukiassian, S. J. Suresha, J. C. Duda, B. M. Foley, C.-H. Lee, Y. Zhu, A. W. Lichtenberger, J. E. Moore, D. A. Muller, D. G. Schlom, P. E. Hopkins, A. Majumdar, R. Ramesh and M. A. Zurbuchen, "Crossover from incoherent to coherent phonon scattering in epitaxial oxide superlattices," *Nature Materials* **13**, 168-172 (2014).
22. S. Y. Ren and J. D. Dow, "Thermal conductivity of superlattices," *Physical Review B* **25**, 3750-3755 (1982).
23. R. Dingle, H. L. Störmer, A. C. Gossard and W. Wiegmann, "Electron mobilities in modulation□doped semiconductor heterojunction superlattices," *Applied Physics Letters* **33**, 665-667 (1978).
24. H. L. Störmer, R. Dingle, A. C. Gossard, W. Wiegmann and M. D. Sturge, "Two-dimensional electron gas at a semiconductor-semiconductor interface," *Solid State Communications* **88**, 933-937 (1993).
25. A. Samarelli, L. F. Llin, S. Cecchi, J. Frigerio, T. Etzelstorfer, E. Müller, Y. Zhang, J. R. Watling, D. Chrastina, G. Isella, J. Stangl, J. P. Hague, J. M. R. Weaver, P. Dobson and D. J. Paul, "The thermoelectric properties of Ge/SiGe modulation doped superlattices," *Journal of Applied Physics* **113**, 233704 (2013).
26. S. R. Wood, D. R. Merrill, G. Mitchson, A. C. Lygo, S. R. Bauers, D. M. Hamann, D. R. Sutherland, J. Ditto and D. C. Johnson, "Modulation Doping in Metastable Heterostructures via Kinetically Controlled Substitution," *Chemistry of Materials* **29**, 773-779 (2017).
27. Y.-L. Pei, H. Wu, D. Wu, F. Zheng and J. He, "High Thermoelectric Performance Realized in a BiCuSeO System by Improving Carrier Mobility through 3D Modulation Doping," *Journal of the American Chemical Society* **136**, 13902-13908 (2014).
28. B. Yu, M. Zebarjadi, H. Wang, K. Lukas, H. Wang, D. Wang, C. Opeil, M. Dresselhaus, G. Chen and Z. Ren, "Enhancement of Thermoelectric Properties by Modulation-Doping in Silicon Germanium Alloy Nanocomposites," *Nano Letters* **12**, 2077-2082 (2012).
29. M. Zebarjadi, G. Joshi, G. Zhu, B. Yu, A. Minnich, Y. Lan, X. Wang, M. Dresselhaus, Z. Ren and G. Chen, "Power Factor Enhancement by Modulation Doping in Bulk Nanocomposites," *Nano Letters* **11**, 2225-2230 (2011).

30. P. L. Kapitza, "The study of heat transfer in Helium II," *Zhurnal eksperimentalnoi i teoreticheskoi fiziki* **11**, 1-31 (1941).
31. E. T. Swartz and R. O. Pohl, "Thermal boundary resistance," *Reviews of Modern Physics* **61**, 605-668 (1989).
32. P. E. Hopkins, "Thermal transport across solid interfaces with nanoscale imperfections: Effects of roughness, disorder, dislocations, and bonding on thermal boundary conductance," *ISRN Mechanical Engineering* **2013**, 682586 (2013).
33. B. F. Donovan, B. M. Foley, J. F. Ihlefeld, J.-P. Maria and P. E. Hopkins, "Spectral phonon scattering effects on the thermal conductivity of nano-grained barium titanate," *Applied Physics Letters* **105**, 082907 (2014).
34. L. Chen, J. L. Braun, B. F. Donovan, P. E. Hopkins and S. J. Poon, "Ballistic transport of long wavelength phonons and thermal conductivity accumulation in nanograined silicon-germanium alloys," *Applied Physics Letters* **111**, 131902 (2017).
35. B. M. Foley, H. J. Brown-Shaklee, J. C. Duda, R. Cheaito, B. J. Gibbons, D. Medlin, J. F. Ihlefeld and P. E. Hopkins, "Thermal conductivity of nano-grained $SrTiO_3$ thin films," *Applied Physics Letters* **101**, 231908 (2012).
36. A. D. McConnell and K. E. Goodson, "Thermal conduction in silicon micro- and nanostructures," *Annual Review of Heat Transfer* **14**, 129-168 (2005).
37. B. F. Donovan, E. Sachet, J.-P. Maria and P. E. Hopkins, "Interplay between mass-impurity and vacancy phonon scattering effects on the thermal conductivity of doped cadmium oxide," *Applied Physics Letters* **108**, 021901 (2016).
38. E. Sachet, C. T. Shelton, J. S. Harris, B. E. Gaddy, D. L. Irving, S. Curtarolo, B. F. Donovan, P. E. Hopkins, P. A. Sharma, A. L. Sharma, J. F. Ihlefeld, S. Franzen and J. P. Maria, "Dysprosium-doped cadmium oxide as a gateway material for mid-infrared plasmonics," *Nature Materials* **14**, 414-420 (2015).
39. E. L. Runnerstrom, K. P. Kelley, E. Sachet, C. T. Shelton and J.-P. Maria, "Epsilon-near-Zero Modes and Surface Plasmon Resonance in Fluorine-Doped Cadmium Oxide Thin Films," *ACS Photonics* **4**, 1885-1892 (2017).
40. A. Poddubny, I. Iorsh, P. Belov and Y. Kivshar, "Hyperbolic metamaterials," *Nature Photonics* **7**, 948 (2013).
41. A. J. Hoffman, L. Alekseyev, S. S. Howard, K. J. Franz, D. Wasserman, V. A. Podolskiy, E. E. Narimanov, D. L. Sivco and C. Gmachl, "Negative refraction in semiconductor metamaterials," *Nature Materials* **6**, 946 (2007).
42. Z. Sun, A. Martinez and F. Wang, "Optical modulators with 2D layered materials," *Nature Photonics* **10**, 227 (2016).
43. A. Mazuelas, R. Hey, B. Jenichen and H. T. Grahn, "Alternating Be and C doping for strain compensated GaAs/AlAs distributed Bragg reflectors," *Applied Physics Letters* **70**, 2088-2090 (1997).
44. K. P. Kelley, E. Sachet, C. T. Shelton and J.-P. Maria, "High mobility yttrium doped cadmium oxide thin films," *APL Materials* **5**, 076105 (2017).
45. D. Strauch, "CdO: lattice parameters," in *New Data and Updates for several III-V (including mixed crystals) and II-VI Compounds*, U. Rössler ed., 77-79 (Springer Berlin Heidelberg, 2012).
46. See Supplemental Material at [URL will be inserted by publisher] for details of time domain thermoreflectance measurements, dislocation density effects on CdO thermal conductivity and thermal boundary conductances, validation of seris resistor analysis of

thermal transport on the MoDECs, spatial segregation of free carriers in the MoDECs, Hall effect measurements, and mid-infreared reflectivity measurements.

47. J. Nishitani, K. M. Yu and W. Walukiewicz, "Charge transfer and mobility enhancement at CdO/SnTe heterointerfaces," *Applied Physics Letters* **105**, 132103 (2014).
48. B. Arnaudov, T. Paskova, S. Evtimova, E. Valcheva, M. Heuken and B. Monemar, "Multilayer model for Hall effect data analysis of semiconductor structures with step-changed conductivity," *Physical Review B* **67**, 045314 (2003).
49. D. G. Cahill, "Analysis of heat flow in layered structures for time-domain thermoreflectance," *Review of Scientific Instruments* **75**, 5119-5122 (2004).
50. A. J. Schmidt, "Pump-probe thermoreflectance," *Annual Review of Heat Transfer* **16**, 159-181 (2013).
51. P. E. Hopkins, J. R. Serrano, L. M. Phinney, S. P. Kearney, T. W. Grasser and C. T. Harris, "Criteria for cross-plane dominated thermal transport in multilayer thin film systems during modulated laser heating," *Journal of Heat Transfer* **132**, 081302 (2010).
52. B. C. Gundrum, D. G. Cahill and R. S. Averback, "Thermal conductance of metal-metal interfaces," *Physical Review B* **72**, 245426 (2005).
53. P. E. Hopkins, T. E. Beechem, J. C. Duda, J. L. Smoyer and P. M. Norris, "Effects of subconduction band excitations on thermal conductance at metal-metal interfaces," *Applied Physics Letters* **96**, 011907 (2010).
54. V. Rawat, Y. K. Koh, D. G. Cahill and T. D. Sands, "Thermal conductivity of (Zr,W)N/ScN metal/semiconductor multilayers and superlattices," *Journal of Applied Physics* **105**, 024909 (2009).
55. P. Jha, T. D. Sands, L. Cassels, P. Jackson, T. Favaloro, B. Kirk, J. Zide, X. Xu and A. Shakouri, "Cross-plane electronic and thermal transport properties of p-type $La_{0.67}Sr_{0.33}MnO_3/LaMnO_3$ perovskite oxide metal/semiconductor superlattices," *Journal of Applied Physics* **112**, 063714 (2012).
56. B. Saha, Y. R. Koh, J. Comparan, S. Sadasivam, J. L. Schroeder, M. Garbrecht, A. Mohammed, J. Birch, T. Fisher, A. Shakouri and T. D. Sands, "Cross-plane thermal conductivity of (Ti,W)N/(Al,Sc)N metal/semiconductor superlattices," *Physical Review B* **93**, 045311 (2016).
57. Y. K. Koh, Y. Cao, D. G. Cahill and D. Jena, "Heat-transport mechanisms in superlattices," *Advanced Functional Materials* **19**, 610-615 (2009).

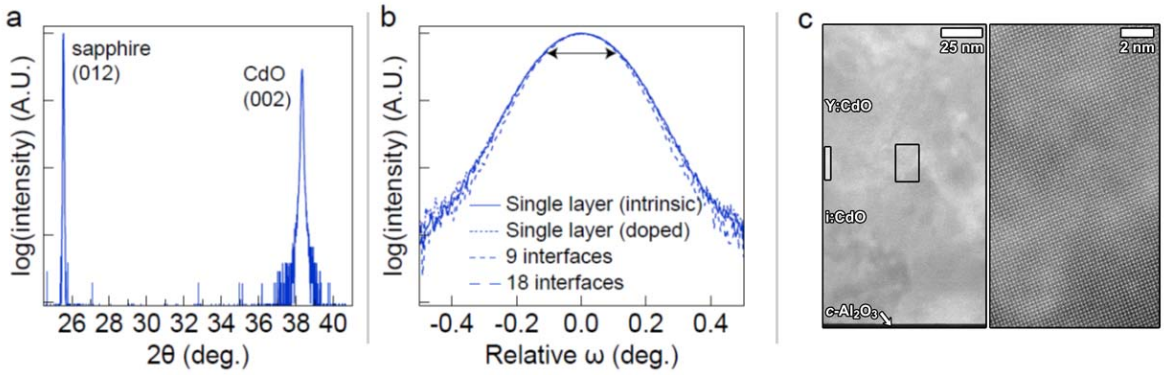

Figure 1. a) $2\theta - \omega$ scan of the (002) peak of the CdO MoDEC on sapphire. b) Rocking curves of the (002) CdO peaks for both single species films and layered MoDECs. There is little to negligible difference in crystallinity between the MoDECs and the CdO films, indicating the MoDECs are single crystalline. c) TEM of 3 layer MoDECs, which shows no lattice distortion at the doped layers, further confirming the highly crystalline quality of these materials. ADF STEM images of an i:CdO/Y:CdO heterostructure interface grown on c-sapphire with no evidence of structural changes induced by doping. The high magnification images were recorded the region of the black rectangular overlay. Doping initiates in the vicinity of the center of the 20 nm long vertically oriented white bar. Taken together, the XRD and TEM characterization suggest that the MoDECs are crystallographically indistinguishable from the homogeneous reference films and the Y-doping and varying modulation periods of the doped layers have negligible impact on the lattice of the films.

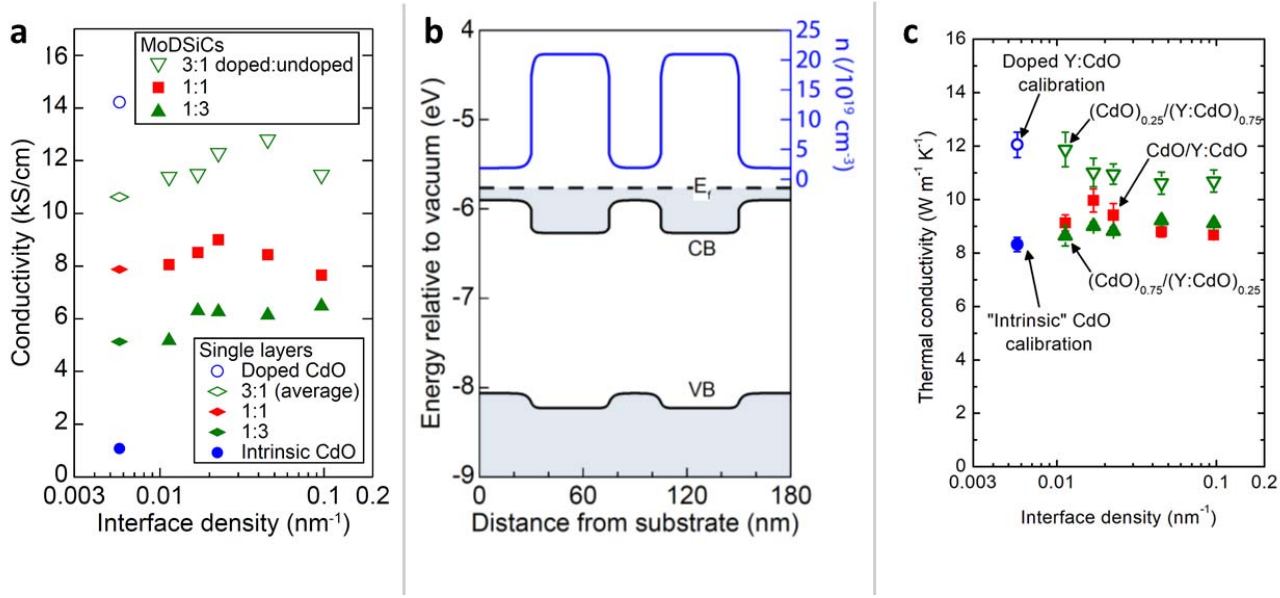

Figure 2. a) Conductivity vs. interfacial density of MoDECs, as measured by Hall measurements. Conductivity scales with overall concentration of carriers. b) Finite-element simulations of Poisson's equation for a five layer CdO MoDEC, showing carriers are well confined to the more highly doped layers. c) Thermal conductivity of all three MoDEC sample series. The thermal conductivities of all MoDECs lie in-between the thermal conductivities of the single species control films.

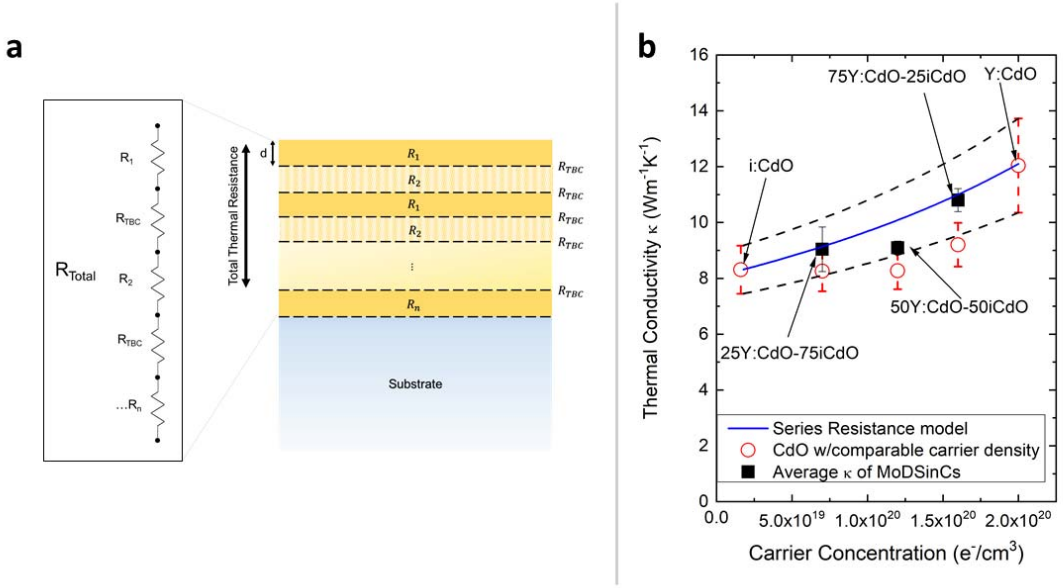

Figure 3. a) Thermal resistance model for a MoDEC. The total thermal resistance of a MoDEC sample (R_{total}) is the sum of the resistances of each layer, and the thermal boundary resistances at the interfaces. b) The blue line is the calculated thermal conductivity of a MoDEC with a concentration of Y:CdO going from 0-100% calculated via. Eq. 2 (where the dotted lines represent the uncertainty of this calculation), assuming R_{int} = 0. The black squares are the average thermal conductivities of the three different MoDEC series. The red circles are the thermal resistance of single species CdO films with a comparable carrier concentration as the corresponding MoDEC. The agreement confirms that the electronic interfaces offer negligible thermal resistance.

Table 1: Nominal thicknesses of each layer in the MoDEC superlattice samples.

	$(CdO)_{0.25}/(Y:CdO)_{0.75}$	$(CdO)_{0.5}/(Y:CdO)_{0.5}$	$(CdO)_{0.75}/(Y:CdO)_{0.25}$
2 layers	Al_2O_3 // 135 nm Y:CdO // 45 nm i-CdO	Al_2O_3 // 90 nm Y:CdO // 90 nm i-CdO	Al_2O_3 // 45 nm Y:CdO // 135 nm i-CdO
3 layers	Al_2O_3 // 22.5 nm i-CdO // 135 nm Y:CdO // 22.5 nm i-CdO	Al_2O_3 // 45 nm i-CdO // 90 nm Y:CdO // 45 nm i-CdO	Al_2O_3 // 67.5 nm i-CdO // 45 nm Y:CdO // 67.5 nm i-CdO
5 layers	Al_2O_3 // [15 nm i-CdO // 67.5 nm Y:CdO] x2 // 15 nm i-CdO	Al_2O_3 // [30 nm i-CdO // 45 nm Y:CdO] x2 // 30 nm i-CdO	Al_2O_3 // [45 nm i-CdO // 22.5 nm Y:CdO] x2 // 45 nm i-CdO
9 layers	Al_2O_3 // [9 nm i-CdO // 33.75 nm Y:CdO] x4 // 9 nm i-CdO	Al_2O_3 // [18 nm i-CdO // 22.5 nm Y:CdO] x4 // 18 nm i-CdO	Al_2O_3 // [27 nm i-CdO // 11.25 nm Y:CdO] x4 // 27 nm i-CdO
18 layers	Al_2O_3 // [15 nm Y:CdO // 5 nm i-CdO] x 9	Al_2O_3 // [10 nm Y:CdO // 10 nm i-CdO] x 9	Al_2O_3 // [5 nm Y:CdO // 15 nm i-CdO] x 9